

The ATLAS Tile Calorimeter performance and its upgrade towards the High Luminosity Large Hadron Collider

R. P. McKenzie*, on behalf of the ATLAS Tile Calorimeter System

School of Physics and Institute for Collider Particle Physics, University of the Witwatersrand, Wits, Johannesburg 2050, South Africa

* ryan.peter.mckenzie@cern.ch



Proceedings for the XXVIII International Workshop
on Deep-Inelastic Scattering and Related Subjects,
Stony Brook University, New York, USA, 12-16 April 2021
doi:[10.21468/SciPostPhysProc.8](https://doi.org/10.21468/SciPostPhysProc.8)

Abstract

The Tile Calorimeter (TileCal) is a sampling calorimeter that forms the central region of the hadronic calorimeter of the ATLAS experiment. This sub-detector is to undergo its Phase-II upgrade during long-shutdown 3, in the years from 2025 to mid 2027, in preparation for the start of operation of the High Luminosity Large Hadron Collider (HL-LHC) in 2027. In this proceeding, an overview of the TileCal HL-LHC on-detector electronics upgrade is provided. The detectors Run-II performance in the cases of EM scale calibration, calorimeter response, cell energy distribution and noise as well as a portion of the 2015-2018 Test-beam campaigns results are examined.



Copyright R. P. McKenzie *et al.*

This work is licensed under the Creative Commons

[Attribution 4.0 International License](https://creativecommons.org/licenses/by/4.0/).

Published by the SciPost Foundation.

Received 11-08-2021

Accepted 04-03-2022

Published 14-07-2022

doi:[10.21468/SciPostPhysProc.8.171](https://doi.org/10.21468/SciPostPhysProc.8.171)



Check for updates

1 Introduction

The TileCal is a sampling calorimeter that forms the central section of the Hadronic calorimeter of the ATLAS experiment [1]. It performs several critical functions within ATLAS such as the measurement and reconstruction of hadrons, jets, hadronic decays of τ -leptons and missing transverse energy. It also contributes to muon identification and provides inputs to the Level 1 calorimeter trigger system.

The detector is located in the pseudorapidity region $|\eta| < 1.7$ ¹ and is partitioned into four barrel regions. Each barrel region consists of 64 wedge shaped modules which cover

¹ATLAS makes use of a right-handed coordinate system with its origin located at the nominal interaction point (IP) in the centre of the detector and the z-axis along the beam pipe. The x-axis points from the IP to the centre of the LHC ring, and the y-axis points upwards. Cylindrical coordinates (r, ϕ) are used in the transverse plane, where ϕ is defined as the azimuthal angle around the z-axis. The pseudorapidity is defined in terms of the polar angle θ as $\eta = -\ln \tan(\theta/2)$.

$\Delta\phi \sim 0.1^1$ and are composed of plastic scintillator tiles, functioning as the active media, inter-spaced by steel absorber plates.

In the third quarter of 2027 the start of the operation of the HL-LHC is planned with a foreseen peak luminosity of $5 \times 10^{34} \text{ cm}^{-2} \text{ s}^{-1}$ [2]. The resulting environment has necessitated the development of new electronics, both on and off detector, to ensure the continued peak performance of the detector. The new electronics need to meet the requirements of a 1 MHz trigger for the Level 1 trigger system, higher resistance to ambient radiation exposure, and improved performance under high pileup conditions.

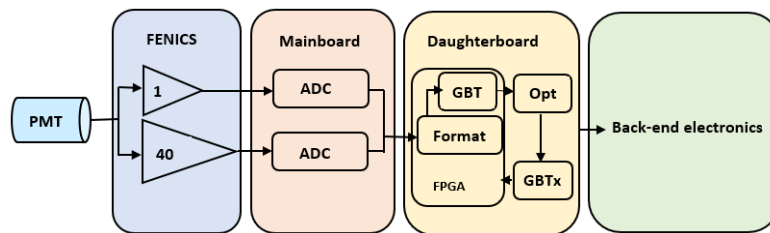


Figure 1: The TileCal HL-LHC front-end readout chain.

2 HL-LHC TileCal Front-End

In order to meet the requirements of the HL-LHC a completely new read-out architecture, as illustrated in Figure 1, will be implemented within TileCal. In the new Trigger and Data Acquisition (TDAQ) architecture the output signals of the Tile detector cells will be digitized, by the on-detector front-end electronics, and then transferred off-detector for every bunch crossing for further processing.

Mechanics: The on-detector electronics and photo-multiplier tubes of a module as seen in Figure 2 (Right), will be housed within a new drawer configuration. This configuration consists of a three-meter long drawer, known as Super-Drawer (SD), which slides into a girder within the widest section of a module. Each SD is itself composed of either four or three independent Mini-Drawers (MD) depending on whether they are located in the barrel or extended barrel regions, respectively.

Photo-Multiplier Tubes (PMTs) and High Voltage Active Dividers (HVADs): The PMTs, located within the SDs of a module, are responsible for converting scintillation light into analog electrical signals which are then sent to the next stage of the signal chain. Most cells are read out by two PMTs, accounting for 9856 read-out channels in total corresponding to 5182 cells. A total of 768 PMTs, which are located in the most exposed regions will be replaced due to aging. An HVAD is located at the end of every PMT. The function of which is to divide the input high voltage amongst the PMT dynodes utilizing active components thereby improving the linearity of the response.

Front End board for the New Infrastructure with Calibration and signal Shaping (FENICS): Located atop and attached to every HVAD is a FENICS. A FENICS is a readout electronics board that is responsible for the amplification and shaping of the analog signals received from a PMT. The two main roles of a FENICS are: to read the fast signals using two gains and to read the average current using six gains. A FENICS also contains two calibration systems, namely

the charge injection system, utilized for physics signal readout calibration, and the current injection system for the integrator readout.

MainBoard (MB) and DaughterBoard (DB): A MB is located within each MD of TileCal. A single MB interfaces with twelve FENICS and one DB. A MB digitizes the low and high gain signals received from the FENICS which are then sent to its associated DB. The DBs are the primary interface between the on- and off-detector electronics and are mounted on top of every MB. A DB transmits detector data to the off-detector electronics, receives and distributes LHC clocks, configurations as well as slow-control commands.

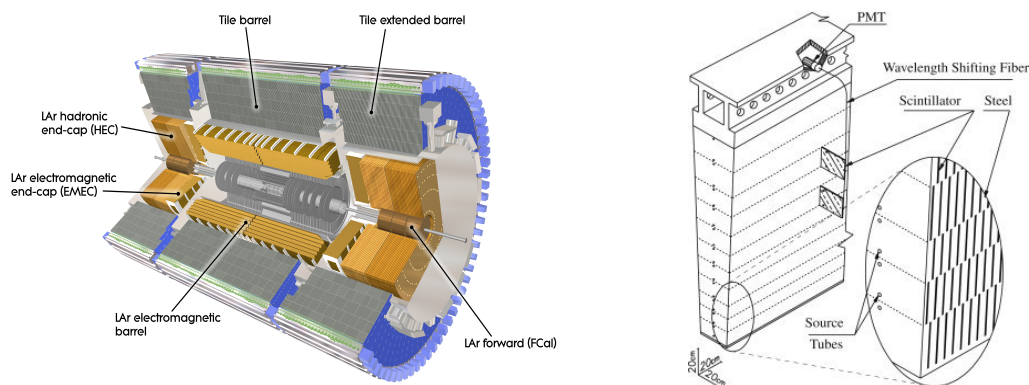


Figure 2: A computer generated image of the ATLAS calorimeter (Left) [4]. An individual module (Right) [3].

High Voltage (HV) distribution system: The HV distribution system provides regulated high voltage power to the HVADs. It consists of off-detector HV Remote-boards that provide the primary HV, received from adjacent HV supply boards to the passive Bus-boards located within the MDs of all modules via 100 m long cables. These Bus-boards then distribute the HV power to the HVADs.

Low Voltage (LV) system: The LV system provides low-voltage power to the front-end electronics located within a SD. The system is functionally separated into on and off-detector electronics. The off-detector electronics are comprised of Auxiliary boards, that provide on/off control of the individual Bricks within a Low Voltage Power Supply (LVPS), as well as 200 VDC power supplies. A LVPS, of which one is located on the end of every SD, is comprised of eight transformer-coupled buck converters that function to step down the 200 VDC, received from the off-detector power supplies to 10 VDC. The 10 VDC power is then routed to point-of-load regulators which perform the final stepping down to that required by the local circuitry within the SDs. There is also an Embedded Local Monitoring Board, that digitizes the signals received from the Bricks which are then sent via CAN bus to the detector control system, and a single fuse board located within a LVPS.

3 Run-II Performance

The response of each detector channel, of which there are typically two per read-out cell, is reconstructed and the resulting signal is calibrated to the ElectroMagnetic (EM) scale. The sum of the channel responses is then calibrated to measure the energy deposited by a particle.

Isolated muons from cosmic rays are used to study the EM scale in-situ as well as the inter-calibration between different layers and regions within the detector. The method applied in the study of 2015 cosmic ray data utilizes the calorimeter cell response and the track path-length to investigate the uniformity of cell response. Muon tracks are extrapolated through TileCal, the distance traversed (dx) and energy deposited (dE) in a

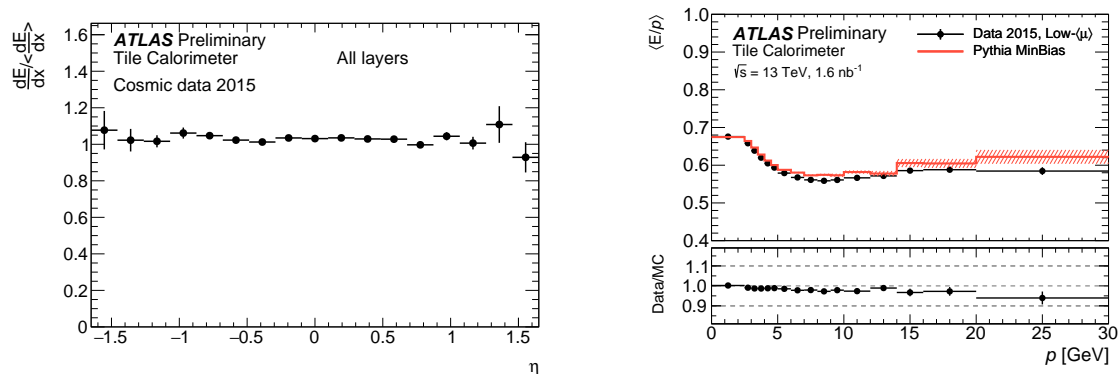


Figure 3: Ratios of the truncated means of the distributions of the energy deposited in the layer cells by cosmic-ray muons per unit of path length, dE/dx , obtained using 2015 data as a function of the pseudorapidity, η (Left) [6]. The calorimeter response to single isolated charged hadrons, characterised by the mean of the energy over momentum $\langle E/p \rangle$ as a function of momentum, integrated over the pseudo-rapidity and ϕ coverage of the calorimeter as measured by the ATLAS Tile Calorimeter using 1.6 fb^{-1} of proton-proton collision data at 13 TeV collected in 2015 (Right) [6].

cell are used to estimate the muon energy loss per unit distance, $\Delta E/\Delta x$. The stability or uniformity is expressed as the normalized truncated mean of dE/dx . The normalized mean of dE/dx is the ratio of dE/dx to the average dE/dx for all the cells. The uniformity of response is presented as a function of pseudorapidity, η , in Figure 3 (Left). We observe that the cell response non-uniformity in pseudorapidity is better than 5%.

The calorimeter energy response can be probed using single hadrons. This as hadrons deposit more energy within the hadronic calorimeter as compared to muons and therefore the response to higher energies can be investigated. The energy response to single isolated charged hadrons is evaluated in-situ from the ratio of a hadron’s energy, E , as measured by TileCal, to the associated isolated track momentum, p , as measured by the ATLAS inner detector system. The track momentum serves as an excellent substitute for the correct energy measurement of the isolated charged hadron, since its uncertainty in the momentum range considered here, is much smaller than the uncertainty on the energy measurement in the calorimeter. A distribution of the average $\langle E/p \rangle$ as a function of track momentum including statistical uncertainties is shown in Figure 3 (Right). Data and Monte Carlo (MC) simulation agree within 5% with the mean $\langle E/p \rangle$ falling below 1 due to the non-compensating nature of TileCal.

A good description of the cell energy distribution, as well as the noise, is crucial for the construction of topoclusters that are used for jet and missing transverse energy reconstruction. With this in mind the distribution of the energy deposited within the cells from collision data at $\sqrt{s} = 13$ and 0.9 TeV, superimposed with the minimum bias MC and the electronic noise (blue-shaded area) corresponding to electronic noise was created. This yielded good agreement between data and MC in the cell energy distribution, as seen in Figure 4.

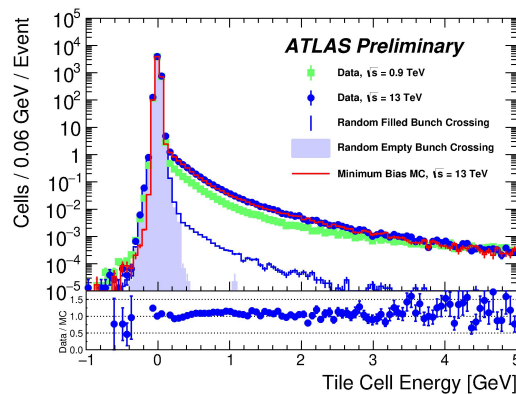


Figure 4: Distributions of the energy deposited in the TileCal cells from collision data at $\sqrt{s} = 13$ and 0.9 TeV superimposed with Pythia minimum bias MC and randomly triggered events from filled and empty bunch crossings [6].

4 Test Beam Performance

The TileCal Test-Beam (TB) apparatus consists of TileCal modules equipped with Phase-II upgrade electronics stacked atop a scanning table, that allows for the rotation of the apparatus with respect to the stationary beam line, together with modules equipped with the legacy system as well as all the required control and power electronics [3]. This apparatus was exposed to different particles and energies at the Super Proton Synchrotron beam-line in test-beam campaigns undertaken from 2015 to 2018. The purpose of which was to test and validate the proposed HL-LHC TileCal electronics. The data and subsequent studies have yielded numerous interesting results, three of which shall be presented.

In Figure 5 (Left), the distributions obtained using experimental and simulated results, obtained using Geant 4.10.1 [8], in the case of electron beams of 20, 50, and 100 GeV incident in the A-4 cell [3] at 20° with respect to the beam line are shown. For a given beam energy the experimental and the simulated data agree well proving the purity of the selected experimental electron samples.

The Fractional resolution, $R^{\sigma_{raw}} = \sigma_{raw}/E_{beam}$, measured (red circles) and predicted by MC simulation (black squares) as a function of $1/\sqrt{E_{beam}}$ obtained in the case of proton beams is shown in Figure 5 (Right). In which E_{beam} is the energy of the tertiary positive hadron beams incident on the TB modules and σ_{raw} is defined as the energy measurement resolution. The experimental result uncertainties include statistical and systematic effects combined in quadrature. Simulated results show only statistical uncertainties. The red solid (black dashed) curves are fits of the experimental (simulated) data points. The dashed red band takes into account the correlated systematic uncertainties in the case of the experimental determinations. In the bottom of the histogram the fractional deviations $\Delta\sigma_{raw} = \sigma_{raw}/\sigma_{raw_{mc}} - 1$ are illustrated in which a maximum variation of 0.04 is observed. The uncertainties include statistical and systematic effects combined in quadrature.

High energy muons traverse the modules entirely for any angle of incidence, thereby allowing the study of the response throughout their entire volume in detail. The muon-matter interaction is well understood whereby the dominant energy loss process is ionization in which the energy loss is essentially proportional to the muon track path length.

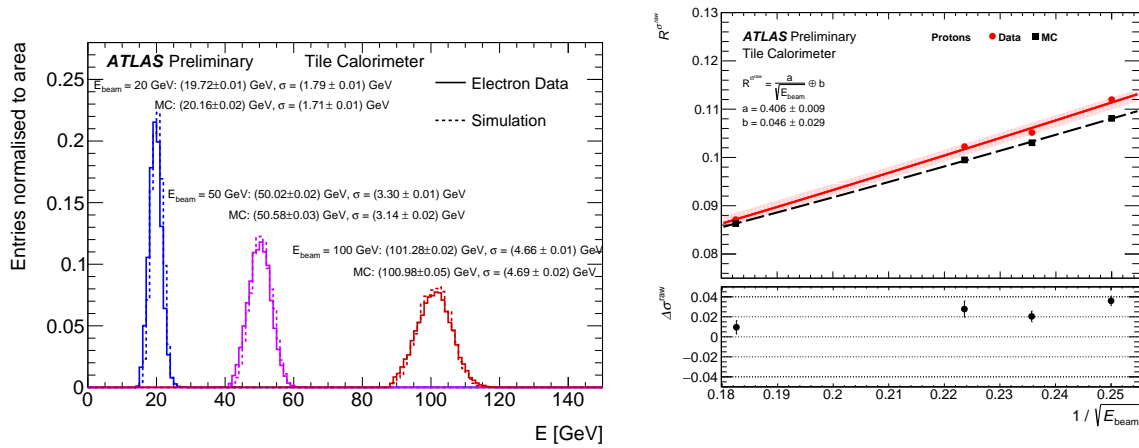


Figure 5: Distributions of the total energy deposited in the calorimeter obtained using electrons beams of 20, 50 and 100 GeV incident in the cell A-4 of the middle layer of the stack at $\theta = 20^\circ$ with respect to the beam line (Left) [5]. The fractional resolution, $R^{raw} = \sigma_{raw}/E_{beam}$, measured and predicted by MC simulation as a function of $1/\sqrt{E_{beam}}$ obtained in the case of proton beams (Right) [5].

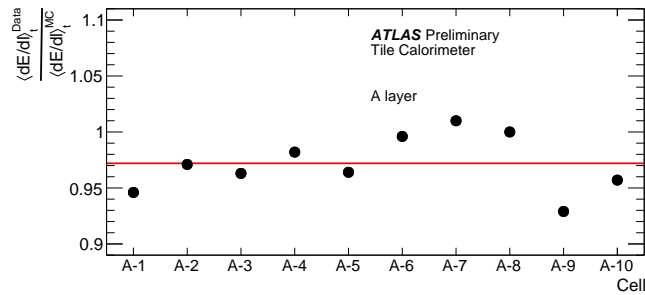


Figure 6: Ratios of the truncated means of the distributions of the energy deposited in the A layer cells per unit of path length obtained using a -90° orientation with respect to the beam line; experimental and simulated muon data as a function of the cell number [5].

In Figure 6 we can observe the ratios of the truncated means of the distributions of the energy deposited in the A layer cells per unit path length obtained using 165 GeV muons at an angle of incidence of -90° ². A layer cells are defined as cells which occupy the narrowest row of a TileCal wedge and are therefore the cells within TileCal which reside closest to the beam line [7]. The experimental and simulated muon data as a function of the cell number was obtained using Geant 4.10.1 [8]. The horizontal red line corresponds to the mean value of the determination. Layer A achieved a uniformity of 1% and a maximum data/MC offset of 3%.

²An angle of incidence of 90° refers to the case whereby the test beam is incident on the side of a module in which the cell numbers are the smallest as opposed to an angle of incidence of -90° which refers to the side in which the cell numbers are the largest. In reference to Figure 6, this can be interpreted as the beam incident on cell A-10 and then traversing the A-layer of the module towards cell A-1.

5 Conclusions

The TileCal has met various performance requirements during its Run-II operation. This was observed via the validation of EM scale settings, probing of its energy response as well as a good description of the cell energy distribution having been obtained amongst numerous other studies.

During the Phase-II research and development phase, the upgrade components have been evaluated by way of numerous successful Test-beam campaigns. Additional Test-Beam campaigns are required as all of the Phase-II upgrade components designs have not been finalized. Upcoming campaigns are to occur in the third quarter of 2021.

Therefore, it can be observed that the TileCal Phase-II upgrade is in a mature state with many of the constituent components being in the final stages of development with some even proceeding to the pre-production and production phases.

Funding information This work is based on research supported in part by the National Research Foundation and the Department of Science and Innovation of South Africa.

Copyright 2021 CERN for the benefit of the ATLAS Collaboration. Reproduction of this article or parts of it is allowed as specified in the CC-BY-4.0 license.

References

- [1] ATLAS Collaboration, *The ATLAS Experiment at the CERN Large Hadron Collider*, J. Inst. **3**, S08003 (2008), doi:[10.1088/1748-0221/3/08/s08003](https://doi.org/10.1088/1748-0221/3/08/s08003).
- [2] *High-Luminosity Large Hadron Collider (HL-LHC)* official web page (2020), <https://hilumilhc.web.cern.ch/content/hl-lhc-project>.
- [3] ATLAS Collaboration, *Technical Design Report for the Phase-II Upgrade of the ATLAS Tile Calorimeter*, ATLAS-TDR-028 (2017), <https://cds.cern.ch/record/2285583>.
- [4] ATLAS Collaboration, *Computer Generated image of the ATLAS calorimeter* (2008), <https://cds.cern.ch/record/1095927>.
- [5] ATLAS Collaboration, *Approved Tile Calorimeter Plots (Cosmics/Single beam, Calibrations, Testbeam, Upgrades)*, <https://twiki.cern.ch/twiki/bin/view/AtlasPublic/ApprovedPlotsTile>.
- [6] ATLAS Collaboration, *Public Tile Calorimeter Plots for Collision Data*, <https://twiki.cern.ch/twiki/bin/view/AtlasPublic/TileCaloPublicResults>.
- [7] J. Abdallah et al., *Study of energy response and resolution of the ATLAS Tile Calorimeter to hadrons of energies from 16 to 30 GeV*, Eur. Phys. J. C **81**, 549 (2021), doi:[10.1140/epjc/s10052-021-09292-5](https://doi.org/10.1140/epjc/s10052-021-09292-5).
- [8] S. Agostinelli et al., *Geant 4 – A simulation toolkit*, Nucl. Instr. Meth. Phys. A **506**, 250 (2003), doi:[10.1016/S0168-9002\(03\)01368-8](https://doi.org/10.1016/S0168-9002(03)01368-8).